International Journal of Biological Macromolecules 199 (2022) 318–330

Contents lists available at ScienceDirect

International Journal of Biological Macromolecules

journal homepage: www.elsevier.com/locate/ijbiomac

Epichlorohydrin and tripolyphosphate-crosslinked chitosan–kaolin composite for Auramine O dye removal from aqueous solutions: Experimental study and DFT calculations

Zeynep Mine Şenol [a,*], Serap Çetinkaya [b], Ali Fazıl Yenidünya [b], Faika Başoğlu-Ünal [c], Abdulilah Ece [d,*]

[a] Sivas Cumhuriyet University, Zara Vocational School, Department of Food Technology, 58140 Sivas, Turkey
[b] Sivas Cumhuriyet University, Science Faculty, Department of Molecular Biology and Genetics, 58140 Sivas, Turkey
[c] European University of Lefke, Faculty of Pharmacy, Department of Pharmaceutical Chemistry, Northern Cyprus, TR-10 Mersin, Turkey
[d] Biruni University, Faculty of Pharmacy, Department of Pharmaceutical Chemistry, 34010 İstanbul, Turkey

ARTICLE INFO

Keywords:
Chitosan
Kaolin
Dye removal
DFT calculations
Mechanism

ABSTRACT

Chitosan (Ch, a natural polymer) and kaolin (K, a natural mineral) composite (Ch-K) was produced with the help of two crosslinkers, epichlorohydrin and tripolyphosphate, and then moulded into uniform beads in tripolyphosphate solution. The synthesis was proved by the analyses involving FT-IR and SEM-EDX. The beads were then used as the natural adsorbent for removal of the auramine O (AO), a frequently-used industrial dye, in aqueous solutions. Adsorbent performance of the Ch-K composite for AO dye molecules was optimized: 500 mg L^{-1} at pH 7.5 at 25 °C. The Langmuir model found 0.118 mol kg^{-1} for the maximum adsorption capacity of the Ch-K and the D-R isotherm model showed that the nature of the adsorption process was physical. Kinetics of the adsorption could be explained by using both IPD (intraparticle diffusion) and PSO (pseudo second order) models. Thermodynamic parameters demonstrated that the behaviour of the adsorption was an endothermic and spontaneous. The activity of the composite adsorbent was recovered (88%) after the five sequential adsorption/desorption cycles. Supported by experimental findings, the results obtained from *in silico* modeling at M06-2X/6–31+G (d,p) level helped hypothesise a mechanism for the formation of the Ch-K composite, and shed some light onto the adsorption behaviour of AO dye by assuming several favourable intermolecular interactions.

1. Introduction

A majority of wastewater comes from extensive use of organic dyes and other pollutants in paper, pharmacy, rubber and textile industries [1,2]. The release of wastewater into natural water bodies can cause dramatical effects by changing color, pH or oxygen concentration which may result in serious health and environmental issues. Around 15–20% of industrial dyes have been discharged into the environmental water bodies [3,4,5].

Several methods are used in removal of dyes from wastewaters that include but not limited to reverse osmosis, solvent extraction, solid phase ion exchange and chemical precipitation. [6]. Among these methods, adsorption is a physicochemical method mostly used for the removal of dyes from wastewater, which has advantages such as ease of application, efficiency, low cost, environmental friendliness, and high selectivity [7,8,9,10]. The key step in adsorption method is the selection of adsorbent. Otherwise, inefficiency of the adsorbent leads to secondary pollution. Therefore, producing low-cost natural adsorbents that can be easily separated is of vital importance [11]. As a result, research interests are mainly focused on obtaining environmentally friendly adsorbents for removal of dyes from wastewaters.

Chitosan is an environmentally friendly natural polymer material that is highly available, non-toxic, bioactive, biocompatible and biodegradable [12,13,14]. The –OH, $–NH_2$ and $–NH\text{-}CO\text{-}CH_3$ groups in the chitosan chain function as chelating agents for capturing almost all kinds of ions physically or chemically [15,16,17,18,19]. However, the main disadvantage of chitosan-based sorbents is dissolution in acidic solutions [20]. Thus, many researchers have focused on the chemical modification of chitosan aiming to improve both selectivity and mechanical properties in order to remove heavy metals and dyes from

* Corresponding authors.
E-mail addresses: msenol@cumhuriyet.edu.tr (Z.M. Şenol), aece@biruni.edu.tr (A. Ece).

https://doi.org/10.1016/j.ijbiomac.2022.01.008
Received 7 October 2021; Received in revised form 14 December 2021; Accepted 3 January 2022
Available online 11 January 2022

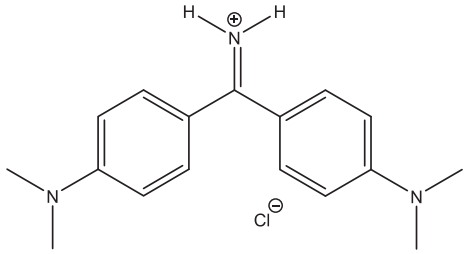

Fig. 1. Chemical structure of Auramine O.

waste water successfully [21]. Numerous cross-linker agents such as tripolyphosphate, epichlorohydrin, and glutaraldehyde can enhance the chitosan stability in the acidic solutions [22].

Natural polymer/clay composites have attracted great interest in recent years as they combine, in their structure, significant physical and chemical properties of inorganic and organic material [23]. Hence, natural inorganic clays have become the flagship of composite manufacturing as they are readily accessible and renewable [24]. Kaolin is one of the frequently used natural inorganic clays, abundantly found in rock crystals [25]. Kaolin, when used alone as an adsorbent and/or composite, is an environmentally friendly material with its significant adsorption capacity, large surface area, simple surface functionalization and high thermal stability [26]. But, the main disadvantage of kaolin adsorbent is that it easily causes agglomeration and coagulation in aqueous solutions. Therefore, a number of modification processes are conducted to improve the kaolin use in aqueous solution. Recent studies have shown that chitosan and kaolin can be used to remove numerous water pollutants, including organic anionic dyes [27], biological pollutants [28], organic cationic dyes [29], and nutrients. These results have indicated that these two components complement one another so as to form multifunctional composite adsorbents. The use of kaolin clay as a filler or modifier of chitosan surfaces has been possible and this process has seemed to have increased the surface area of chitosan and its adsorption properties, thus implicating the possibility for the reduction of both the cost and environmental impact of solid waste disposal activities [2].

In this study, a useful, low-cost, water-insoluble, natural polymer/mineral adsorbent was synthesized from Ch and kaolin (K) and the adsorption of AO dye in aqueous media was explored. To our knowledge, this is the first report on the removal of AO cationic dye using Ch-K composite. Moreover, there is no detailed Ch-K composite formation and adsorption mechanism found in the literature. Therefore, to propose a tentative mechanism, this study also involves quantum mechanical calculations which are among successfully applied *in silico* tools on small molecules and macrosystems [30,31,32]. In order to get accurate results, the selection of computational theory is crucial. Two new hybrid meta exchange-correlation functionals (M06 and M06-2X) were presented and tested by Zhao et al. [33]. We selected M06-2X which, in many cases, have been reported to perform best within the 06 functionals [33]. Based on the experimental and computational results, herein we report the first detailed composite formation and adsorption mechanism which might have a critical impact on the field.

2. Materials and methods

2.1. Chemicals

Kaolin was obtained from Akmin Mining (Ankara, Turkey). The AO (bis [4-(dimethylamino) phenyl] methaniminium chloride) dye was purchased from Merck (Germany) (Fig. 1). Medium molecular weight Ch was used (Sigma-Aldrich, Germany). Other chemicals, sodiumtripolyphosphate (TPP), epichlorohydrin (ECH), HCl, NaOH, KNO_3 and C_2H_5OH were all purchased from Sigma-Aldrich.

2.2. Synthesis of Ch-K

The Ch-K composite was prepared by dissolving 2 g Ch and 2 g K in 30 mL of 5% (*v*/v) aqueous acetic acid solution. The Ch-K mixture was stirred for 2 h until a homogenous mixture was obtained. Then, 4 mL of cross-linker ECH solution was added to the viscous solution. The viscous mixture was left to stand overnight on the bench. The viscous Ch-K mixture was then added dropwise into 0.5 M cross-linker sodium TPP solution to mould it into beads. The synthesized Ch-K composite beads were precipitated and washed five times with distilled water, then the composite was dried at 40 °C and grounded (50 mesh). Finally, a powdered product Ch-K composite was obtained.

2.3. Structural analyses of the Ch-K

Ch-K composite adsorbent was analysed by Fourier Transform Infrared Spectroscopy (FT-IR, Perkin Elmer 400), scanning electron microscopy, and Energy Dispersive X-ray Spectroscopy (TESCAN MIRA3 XMU). The AO dye concentration was measured with a UV–Vis spectrophotometer (T-60, China) at $\lambda = 434$ nm [34].

2.4. Calculation of the electronic properties

Spartan'20 parallel suite from Wavefunction, Inc. Irvine CA, USA, was used for quantum chemical calculations. The molecular geometries of Chitosan (dimeric form) and Auramine O were first optimized at M06-2X/6–31+G(d,p) level of theory. Optimized geometries were verified. Dipole moment (μ), frontier molecular orbital (HOMO-LUMO) energies and other electronic features, (i.e. ionization potential (IP), electron affinity (EA), electronegativity (χ), chemical hardness (η), chemical softness (S), chemical potential (μ), and electrophilicity index (ω), were assessed through the verified geometries.

2.5. Adsorption procedure

The adsorption experiments were carried out using batch methods. 1000 mg L^{-1} AO dye stock solution was prepared. Working solutions were prepared by dilution of the stock AO dye solution with distilled water. The experimental systems included 50 mg of Ch-K composite and 500 mg L^{-1} AO dye at natural pH 7.5. Incubation was carried out for 24 h at 25 °C. The absorbance of the final solutions was read at 434 nm. Eqs. (1) to (3) were used to calculate Adsorption%, Q (mol kg^{-1}) and Desorption% [35].

$$Adsorption\% = \left[\frac{C_i - C_f}{C_i}\right] \times 100 \quad (1)$$

$$Q = \left[\frac{C_i - C_f}{m}\right] \times V \quad (2)$$

$$Desorption\% = \frac{Q_{des}}{Q_{ads}} \times 100 \quad (3)$$

C_i: initial concentration of AO dye (mg L^{-1}); C_f: final concentration of AO dye (mg L^{-1}); V: volume of AO dye (L); m: mass of Ch-K (g); Q_{des}: desorbed AO dye (mol kg^{-1}); and Q_{ads}: adsorbed AO dye (mol kg^{-1}).

2.6. Calculation of adsorption isotherms, kinetics and thermodynamics

Langmuir, Freundlich, and Dubinin-Radushkevich (D-R) isotherm models were used to understand the chemical and physical nature of the adsorption. This model for monolayer assumes that all active sites have the same energy and equal affinity for the molecules to be adsorbed [36]. The general equation of the Langmuir model is shown in Eq. (5).

$$Q = \frac{X_L K_L C_e}{1 + K_L C_e} \quad (5)$$

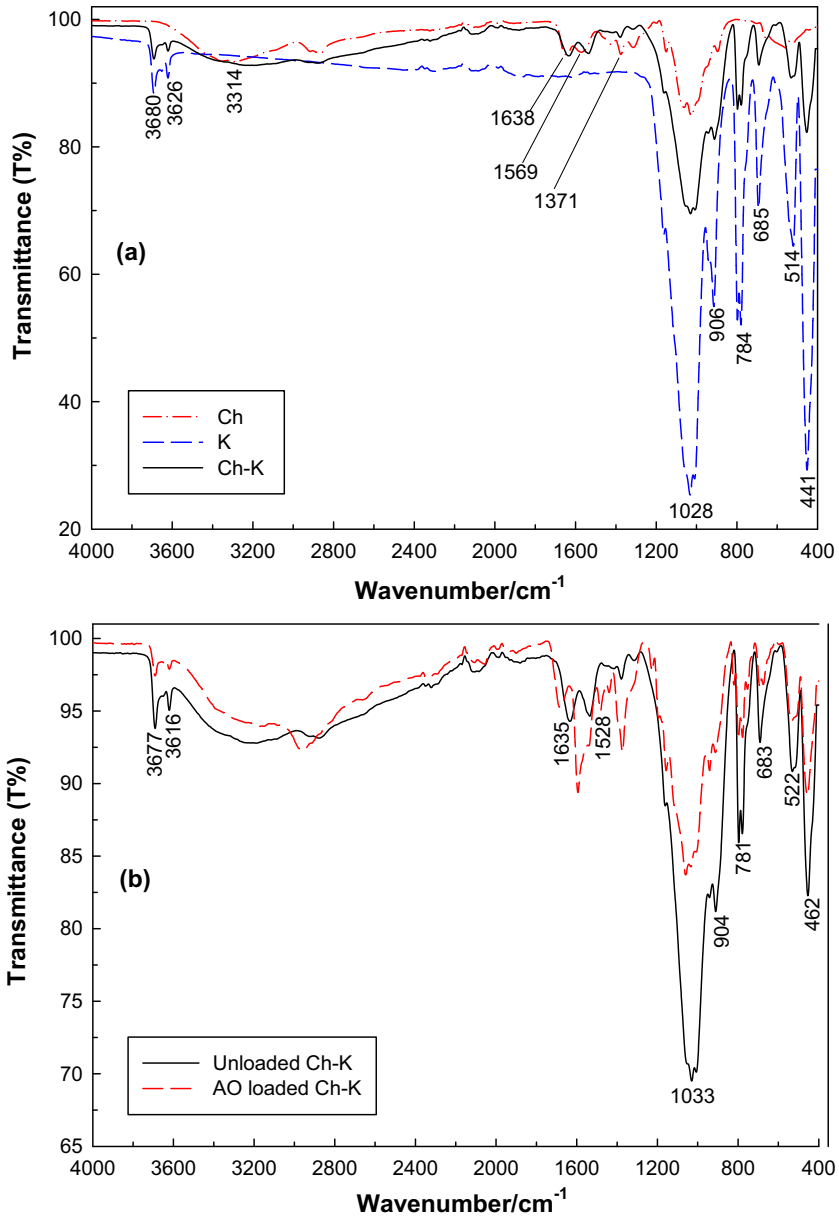

Fig. 2. FT-IR spectra of Ch, K, and Ch-K (a) and unloaded and AO loaded Ch-K (b).

Q (mol kg^{-1}): adsorbed AO; K_L: Langmuir isotherm parameter; C_e: equilibrium concentration (mol L^{-1}); X_L (mol kg^{-1}): maximum adsorption level.

Freundlich model is valid for multilayer adsorptions. It also recognizes that the adsorbent surface is heterogeneous in terms of adsorption areas and energy [37]. The Freundlich equation is expressed as:

$$Q = K_F C_e^{\beta} \tag{6}$$

K_F: Freundlich constant; β: adsorbent surface topology.

The D-R isotherm model is based on the theory of potential exchange on a heterogeneous surface and examines the energetics of the adsorption [38]. D-R model examines the adsorption from the energetic point of view (Eqs. (7)–(9)):

$$Q = Q_{DR} e^{-K_{DR}\varepsilon^2} \tag{7}$$

$$\varepsilon = RTln\left(1 + \frac{1}{C_e}\right) \tag{8}$$

$$E_{DR} = (2K_{DR})^{-0.5} \tag{9}$$

$X_{DR:}$ measured adsorption quantity; R: ideal gas constant (8.314 J mol^{-1} K^{-1}); T: temperature (K); K_{DR}: activity coefficient (mol^2 K J^2); ε: the Polanyi potential calculated using the Eq. (8).

Adsorption energy (E_{DR}) helps us to predict the adsorption mechanism. E_{DR} values between 8 and 16 kj mol^{-1} indicate that the adsorption process should be chemical, and if the values are <8 kj mol^{-1}, it should be physical [39].

Adsorption kinetics were investigated and three well-known kinetic models, PFO- and PSO kinetic models, and IPD model, were applied to the experimental data using the equations given below (Eq. (10)–(12)) [40–42].

$$Q_t = Q_e\left[1 - e^{-k_1 t}\right] \tag{10}$$

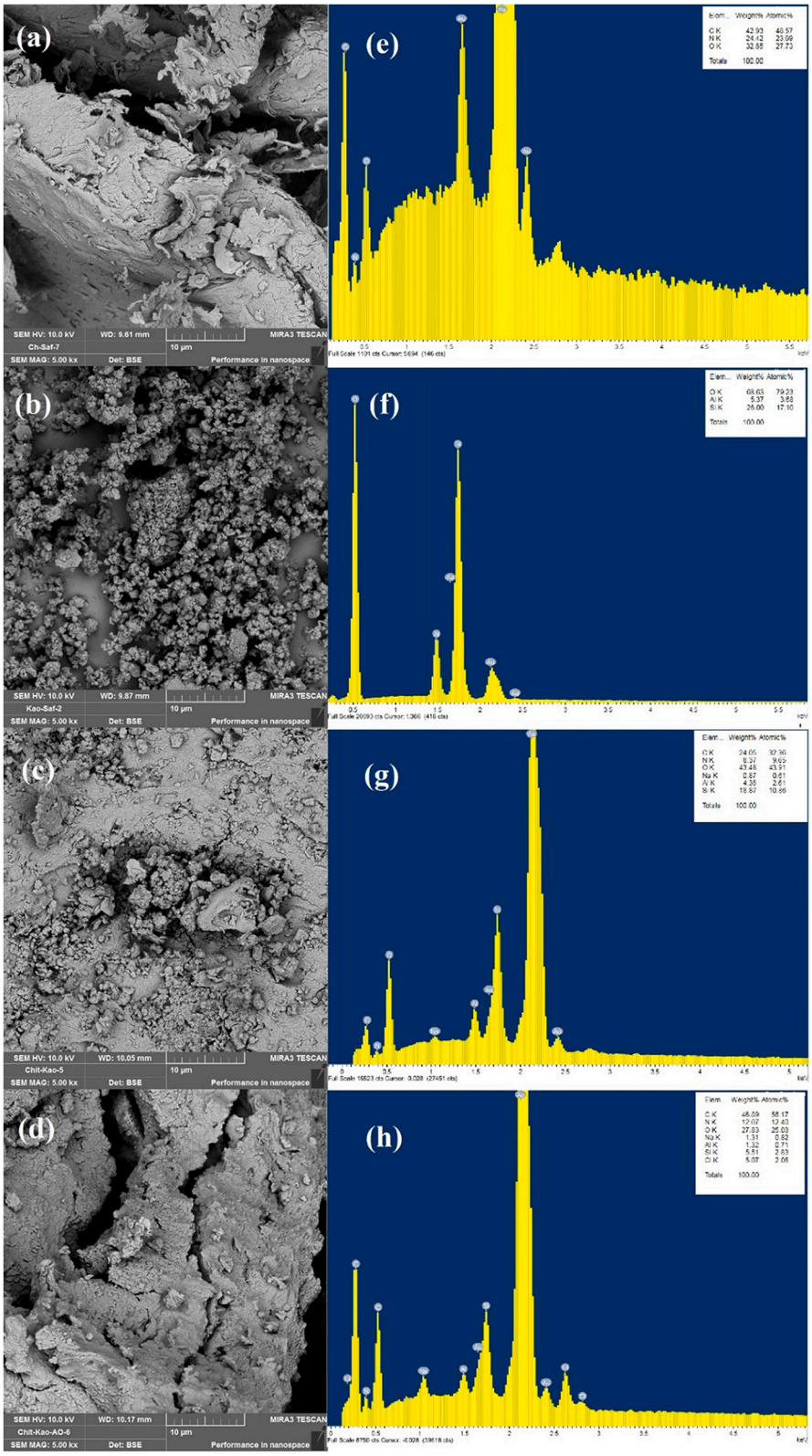

Fig. 3. SEM images of Ch (a), K (b), Ch-K (c) and Ch-K after AO adsorption (d) and EDX spectra of Ch (e), K (f), Ch-K (g) and Ch-K after AO adsorption (h).

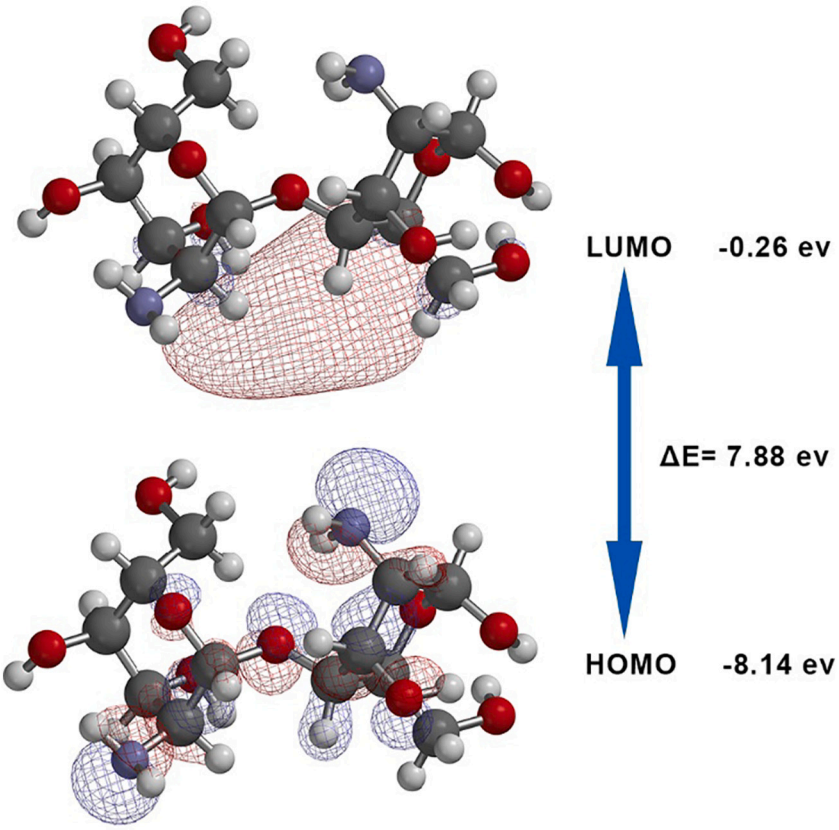

Fig. 4. Frontier molecular orbitals of Ch.

$$Q_t = \frac{t}{\left[\frac{1}{k_2 Q_e^2}\right] + \left[\frac{t}{Q_e}\right]} \quad (11)$$

$$Q_t = k_i t^{0.5} \quad (12)$$

Q_t (mol kg^{-1}): adsorbed quantity with time t (min); Q_e (mol kg^{-1}): adsorbed amount at equilibrium. PFO (min^{-1}) rate constants: k_1, k_2, and k_i; PSO model (mol^{-1} kg min^{-1}), and IPD model (mol^{-1} kg $min^{-0.5}$).

The initial rates for the PFO and PSO models were calculated using Eq. (13)–(14), respectively [43].

$$H_1 = k_1 Q_e \quad (13)$$

$$H_2 = k_2 Q_e^2 \quad (14)$$

The effect of temperature on adsorption, enthalpy (ΔH^0), entropy (ΔS^0), and Gibbs free energy change (ΔG^0) were calculated using the equations below (Eqs. (15)–(18)) [44].

$$K_D = \frac{Q}{C_e} \quad (15)$$

$$\Delta G^0 = -RT\ln K_D \quad (16)$$

$$lnK_D = \frac{\Delta S^0}{R} - \frac{\Delta H^0}{RT} \quad (17)$$

$$\Delta G^0 = \Delta H^0 - T\Delta S^0 \quad (18)$$

3. Results and discussion

3.1. FT-IR, SEM-EDX, and EDX-map analysis

The FT-IR spectra of chitosan, kaolin and Ch-K composite are shown in Fig. 2.

- *Pure Ch FT-IR spectra* (Fig. 2): the hydroxyl (–OH) groups on the surface [45] were represented by a broad band at 3314 cm^{-1}, –NH was observed at 1638 cm^{-1}, the peak at 1569 cm^{-1} was assigned to the NH_2 groups [46], and the COH groups were represented by two peaks at 1371 and 1302 cm^{-1}.
- *FT-IR spectra of kaolin* (Fig. 2): -OH groups in water were represented the peaks at 3680 and 3626 cm^{-1} that formed hydrogen bonds with Si-O-Al of kaolin. Intense Si-O-Si peaks were detected at 1028 and 906 cm^{-1}, the peak seen at 784 cm^{-1} was belong to Si-O-Al; Si—O— Si stretch bands appeared at 685, 514 and 441 cm^{-1} [47].
- *FT-IR spectra of the Ch-K composite* (Fig. 2): A characteristic peak that belongs to the surface –OH groups were observed at 3124 cm^{-1}; chitosan NH_2 groups were seen at 3680, 3619 1645 and 1546 cm^{-1}, and the peak at 1028 cm^{-1} was attributed to the C—N stretching vibration. The stretching vibrations in kaolin at 914 and 784 cm^{-1} were resulted from –Si–OH and –$Al(OH)_3$, while the Si–O–Si stretching vibrations were observed at 678, 533 and 441 cm^{-1}. The presence of both chitosan and kaolin peaks in the FT-IR spectra of the Ch-K alone confirmed the Ch-K synthesis.
- *FT-IR spectra of the unloaded and loaded Ch-K*: Adsorption of the AO dye onto Ch-K composite should results in a change in the magnitude of the peaks which can be easily seen by comparing the FT-IR spectra of unloaded and loaded Ch-K in Fig. 2.

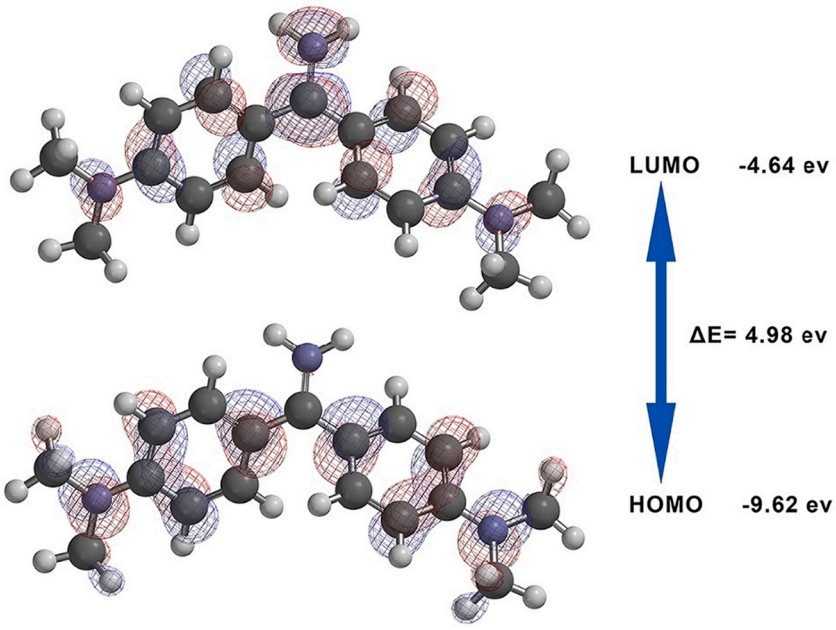

Fig. 5. Frontier molecular orbitals of AO dye.

The surface images of Ch, K and Ch-K were visualised by SEM (Figs. 3 (a-c)). Pure chitosan (Fig. 3a) had a smooth non-porous, indented, microfibrillar, and crystallite surface. Pure kaolin (Fig. 3b), on the other hand, exhibited well-crystallized hexagonal kaolinite morphology with abundant slit- and wedge-shaped pores on a smooth basal surface. Those morphological differences are another prove for the hybrid composite synthesis (Fig. 3c). EDX analysis indicated that pure chitosan contained C, O and N elements (Fig. 3e). A possible kaolinite with the formula $Al_2O_36SiO_2nH_2O$ could be deduced with the elements O, Al, and Si (Fig. 3f). The EDX spectra of the Ch-K composite (Fig. 3g) suggested the presence of the elements C, O, N, Na, Al, and Si, representing both chitosan and kaolin. These findings further proved that the synthesis of Ch-K adsorbent was accomplished.

SEM images of the loaded Ch-K are presented in Fig. 3d. where one could deduce the loaded AO particles on the Ch-K surface. We believe that the observed topology was resulted from the electrostatic interactions and surface complexation between the functional groups on the surface of Ch-K and the AO molecules. EDX results demonstrated that AO loaded Ch-K included C, O, N, Na, Al Si and Cl (Fig. 3h). It also showed the existence of Cl after adsorption (Fig. 3h).

3.2. Computational study

Frontier molecular orbitals (FMO) are two important orbitals (HOMO and LUMO) that give us an idea of the nucleophilicity and the electrophilicity of structures. While HOMO is usually associated with the nucleophilicity or electron-donating ability of the structure; the LUMO indicates the electrophilicity or electron acceptor ability of the structure [48]. A compound with high HOMO energy value can easily donate electrons (ease of oxidation) while low LUMO values are associated with ease of reduction. FMO theory also helps explain the stability and reactivity of dye-adsorbent configurations [49].

Higher energy gaps, ΔE_{GAP} (LUMO-HOMO), result in higher kinetic stability and lower chemical reactivity [50].

A number of quantum molecular descriptors that are critical in evaluating chemical reactivity and stability are all derived from HOMO and LUMO energies. Hence, it was of importance to calculate accurate energies of FMO of Ch and AO to analyse and propose formation of target Ch-K composite and adsorption mechanisms.

According to computational results, FMO calculations showed that HOMO of Ch was localized on amine moieties (Fig. 4). This indicates that a nucleophilic attack by chitosan should be expected to proceed via $-NH_2$ rather than -OH groups. But considering the cyclohexane ring, steric effect will be a barrier for $-NH_2$ for a nucleophilic attack. Thus, attacks through the unpaired electrons of oxygen of hydroxyethyl substituent would be more likely. However, if an acid is being added into a solution of Ch, $-NH_2$ would be protonated first. With all that being said, it can be proposed that mixing Ch polymer with kaolin in the presence of acetic acid results in electrostatic interactions (kaolin-protonated amine) and hydrogen bonding (kaolin-hydroxy methyl of Ch). Afterwards, epichlorohydrin undergoes a nucleophilic attack by oxygen of hydroxymethyl of Ch. This results in a crosslinking between chitosan polymers. To confirm this further, in a separate experiment, methanol was added to the solution at this stage. Indeed, precipitation of polymer was observed. In the last step, electrostatic interactions between tripolyphosphate and chitosan polymer finalize crosslinking procedure that forms uniform beads.

AO dye is a basic and cationic dye. As can be seen Fig. 5, HOMO is located mainly on nitrogen atoms, except quaternary nitrogen where LUMO is spatially localized. Therefore, neutral nitrogens can be regarded as nucleophilic centres, and they can also act as hydrogen bond donors through unpaired electrons with tripolyphosphate, linked to chitosan. Hydrogen bonds are expected to be formed between unpaired electrons of neutral nitrogen with hydroxy groups of tripolyphosphates and a strong electrostatic interaction is also expected between positively charged nitrogen and negatively charged oxygen of tripolyphosphates. In line with the argument made, a tentative mechanism for both Ch-K composite formation and adsorption is proposed in Fig. 6. To the best of our knowledge, this proposed mechanism is the first detailed mechanism reported in the literature based on experimental and computational evidences.

Quantum molecular descriptors are strong tools that are generally referred for evaluating chemical reactivity and stability. Chemical hardness (η) and softness (σ) values can all be calculated from FMO energy values [50,51].

Harder chemical compounds would find significant hindrances when they interact with other molecules. In other words, a compound with high chemical softness can be expected to act as electron donor to a potential acceptor [51]. As can be seen (from Table 1), the chemical hardness of AO dye is lower than that of Ch. Thus, in addition to the

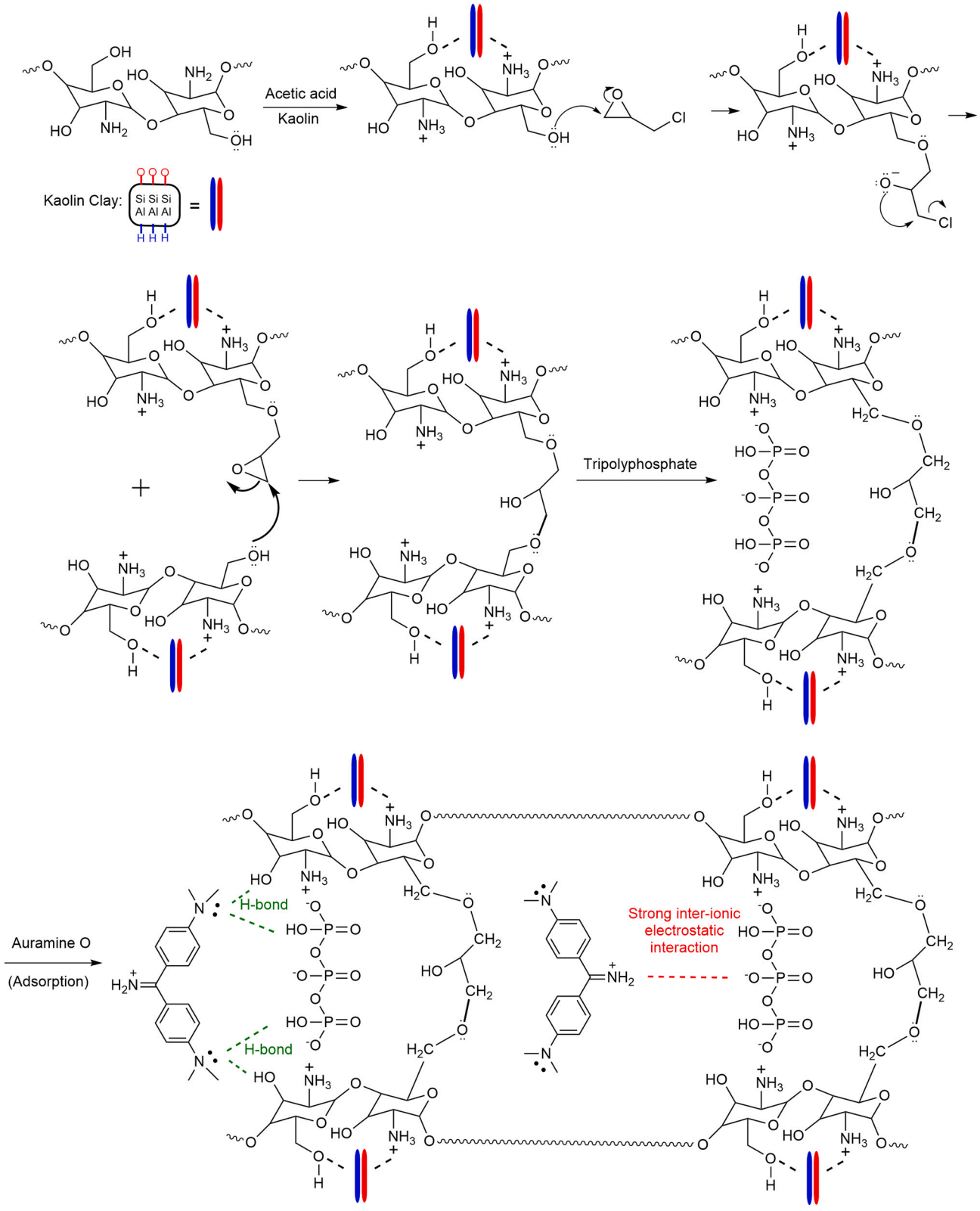

Fig. 6. Proposed Ch-K composite formation and adsorption of AO dye (Only representative interactions are shown).

Table 1
Quantum chemical descriptors of AO dye and Ch calculated at M06-2X/6–31+G (d,p) level of theory.

Calculated properties	Formulas	AO	Ch
HOMO (eV)	–	−9.62	−8.14
LUMO (eV)	–	−4.64	−0.26
ΔE (eV)	LUMO-HOMO	4.98	7.88
Ionization Potential, IP (eV)	Negative of the energy of HOMO	9.62	8.14
Electron Affinity, EA (eV)	Negative of the energy of LUMO	4.64	0.26
Electronegativity, X (eV)	(IP + EA)/2	7.13	4.20
Chemical Hardness, H (eV)	(IP-EA)/2	2.49	4.07
Chemical Softness, S (eV^{-1})	1/η	0.40	0.24

interaction with the tripolyphosphate, we can expect another hydrogen bond formation between electron pairs of AO (H-bond acceptor) and hydrogens of hydroxy groups attached to chitosan (H-bond donor) (Fig. 6).

3.3. Effect of initial pH and PZC on the Ch-K composite

It was observed that adsorption was increased in the high alkaline media (Fig. 7). When the pH was increased from 2 to 8, the adsorption efficiency increased from 5% to 9%. But as the pH increased to 12, the efficiency reached up to 98%. This observed pH dependent adsorption behaviour can be explained by taking into account the proposed mechanism depicted in Fig. 6. Amino and hydroxyl groups are active centres in the Ch-K composite and tripolyphosphate part is also involved in the adsorption of AO dye molecules. At strong acidic pH conditions, negative centers in the cross linked tripolyphosphates are protonated. Therefore, the strong inter-ionic interactions are lost which result in the adsorption capacity of the cationic AO dye molecules to decrease. On the contrary, at large pH values, all hydroxyl groups are expected to be deprotonated. Although the predicted hydrogen bonds will be weakened, number of stronger inter-ionic interactions between AO dye molecules and tripolyphosphate will increase.

The point of zero charge value of Ch-K was found as 5.37 (Fig. 7).

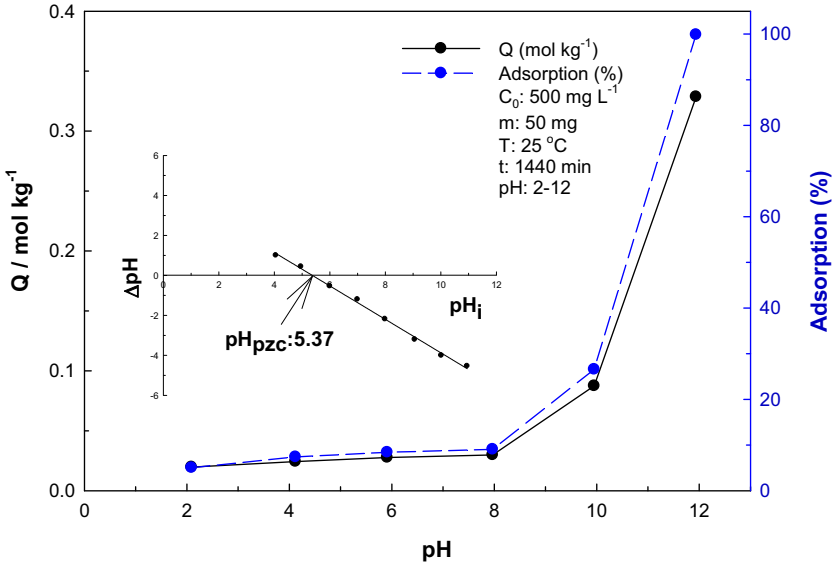

Fig. 7. The effect of pH on the adsorption and pzc of Ch-K.

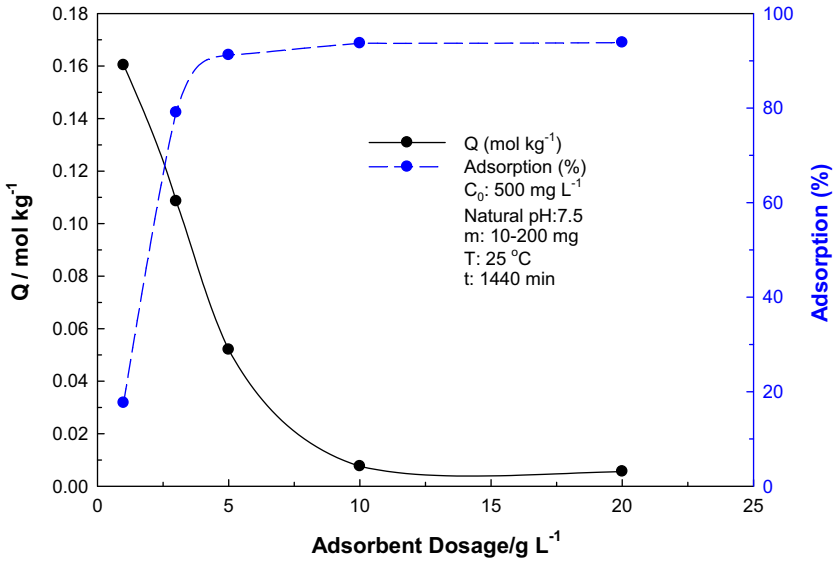

Fig. 8. The effect of adsorbent mass on AO adsorption onto Ch-K.

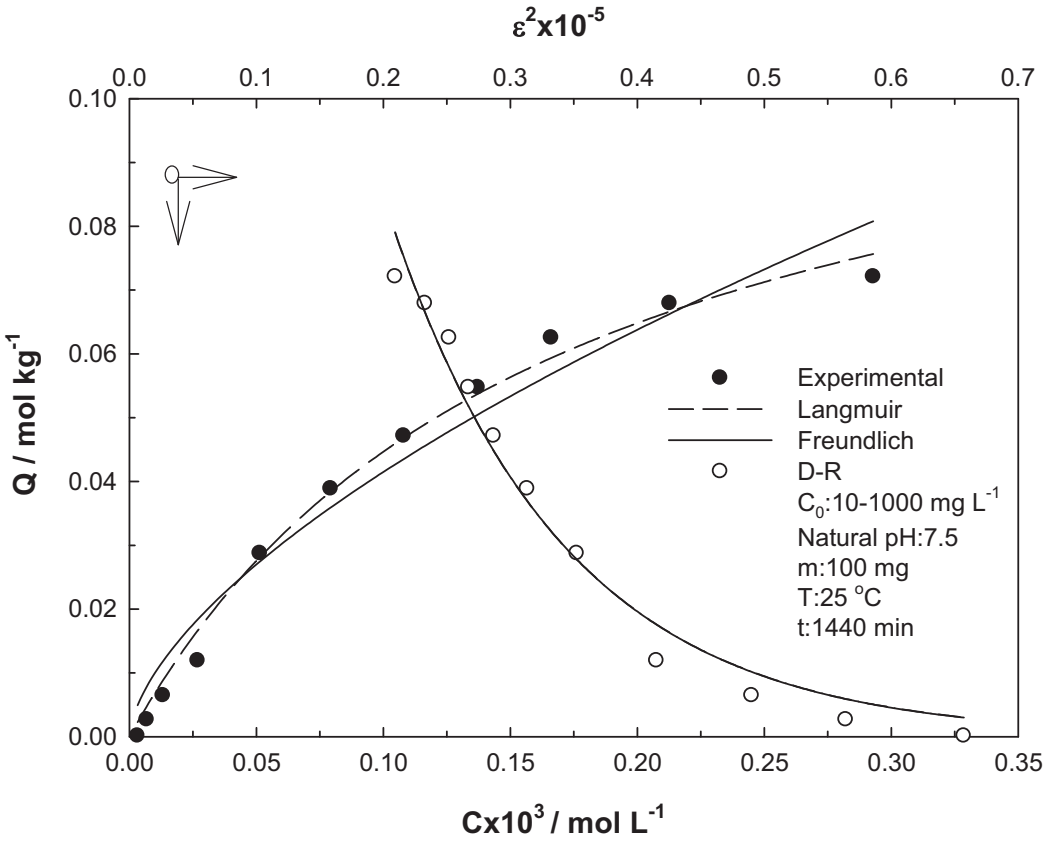

Fig. 9. Experimentally obtained adsorption isotherms of AO onto Ch-K and their compatibility to Langmuir, Freundlich and D-R models.

Table 2
Langmuir, Freundlich and D-R isotherm models' parameters.

Isotherm	Value	R^2
Langmuir		
X_L (mol kg^{-1})	0.118	0.992
K_L (L mol^{-1})	608	
Freundlich		
X_F	3.01	0.963
β	0.620	
D-R		
X_{DR} (mol kg^{-1})	3.65	0.979
$-K_{DR} \times 10^9$/mol^2kJ^{-2}	7.31	
E_{DR}/kJ mol^{-1}	7.3	

This shows that the surface is positive below pH 5.37 and negative above pH 5.37. In other words, at strong acidic pH values, the surface charge became positive (pH < pHpzc), at high pH values the surface charge became negative (pH > pHpzc), resulting in higher adsorption of AO. The natural pH of the cationic AO dye solution was 7.5 and all the adsorption trials were performed at this pH.

The prepared Ch-K composite adsorbent, crosslinked with the ECH and TPP, showed a clear stability at all pH values studied: a noticeable change or damage was not observed during the adsorption processes. In other words, the polymeric adsorbent did not exhibit significant weight loss especially under acidic conditions [52].

3.4. Effect of the adsorbent mass

Adsorbent concentration can often affect the adsorption capacity of a given adsorbent. In the present study, AO concentrations adopted ranged from 0.1 to 20 g L^{-1} (Fig. 8). Adsorption was found to be directly proportional to the concentration of AO until it reached a maximum. At 20 g L^{-1}, approximately 90% of AO was adsorbed (Fig. 8).

Table 3
Comparison of AO dye adsorption on the Ch-K composite with other sorbents.

Sorbent type	pH	Q_{max} (mol kg^{-1})	References
MOF-5/COF	9.5	0.0591	[53]
Gum xanthan-psyllium-cl-poly(acrylic acid-coitaconic acid)	–	0.00540	[54]
Granulated activated carbon ICEG (coconut shell)	9.0	0.396	[55]
Carboxymethyl cellulose grafted poly (methylmethacrylate)/cloisite 30B nanocomposite hydrogels	7.5	0.461	[56]
Poly (acrylic acid)-halloysite nanoclay hydrogel	11.0	0.0142	[57]
Gum xanthan-psyllium with polyacrylic acid-copolyitaconic acid	–	0.00691	[54]
Psidium guava leaves	9.0	0.0257	[58]
De-oiled cotton seed cake biochar	–	0.00428	[59]
Diospyros lotus seed powder	–	0.0889	[60]
Commercial activated carbon	7.0	0.102	[61]
Chitosan-kaolin composite	7.5	0.118	This study

3.5. Modeling of adsorption process

R^2 values obtained from Langmuir and Freundlich models were compared (Fig. 9, Table 2). AO adsorption on Ch-K provided a better fit with the Langmuir model ($R^2 = 0.992$). This indicated that AO molecules formed a monolayer onto the active centers, available on the Ch-K composite. The maximum adsorption capacity and the K_L value were 0.118 mol kg^{-1} and 608 L mol^{-1}, respectively. The comparison between

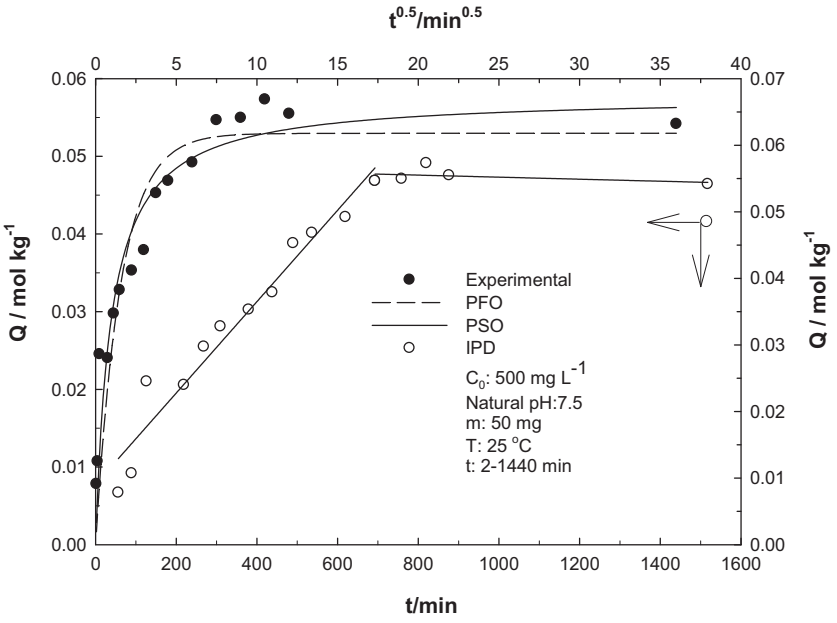

Fig. 10. Compatibility of AO adsorption kinetics to PFO, PSO and IPD models.

Table 4
PFO, PSO and IPD kinetic models' parameters.

Kinetic model	Value	R^2
Pseudo first order		
Q_t/mol kg^{-1}	0.0573	0.866
Q_e/mol kg^{-1}	0.0530	
$k_1 \times 10^3$/dk^{-1}	16.1	
$Hx10^3$/mol kg^{-1} min^{-1}	0.849	
Pseudo second order		
Q_t/mol kg^{-1}	0.0573	0.918
Q_e/mol kg^{-1}	0.0578	
$k_2 \times 10^3$/mol^{-1}kg min^{-1}	450	
$Hx10^3$/mol kg^{-1} min^{-1}	1.50	
Intra particle diffusion		
$k_i \times 10^3$/mol kg^{-1} $min^{-0.5}$	9.06	0.949

the maximum adsorption capacities of Ch-K composite adsorbent for AO dye, and those of the other sorbents reported in the literature are provided in Table 3. The adsorption capacity for most of the adsorbent materials studied are relatively low in comparison to our results. X_F, a measure of adsorption capacity, was calculated to be 3.01 using the Freundlich isotherm model. Beta surface heterogeneity was 0.620. This showed that the conditions were favourable for the adsorption. The adsorption energy, 7.3 kJ mol^{-1}, derived by the D-R model, suggested that the nature of the adsorption was physical.

3.6. Effect of contact time

The data from pseudo first order (PFO), pseudo second order (PSO) and intra particle diffusion (IPD) models (Fig. 10, Table 4) indicated that the adsorption rate was fast initially, when all the active sites were empty on the surface of the composite. After the 6 h, an equilibrium plateau was reached and maintained until the 24 h. This plateau indicated the saturation of the Ch-K active sites with the dye molecules and a slower IPD. The coefficient of determination (R^2) proved that the experimental data obeyed the PSO model (Table 4). Moreover, the fact that theoretical Q_t and experimental Q_e values are very close to each other also supports this finding. The IPD model produced two distinct lines, in the graph. On the basis of this finding, it can be inferred that the adsorption involved both the surface and IPD and this behaviour can only be explained by adopting both the PSO- and IPD models.

3.7. Effect of temperature

In order to see the thermodynamic behaviour of adsorption in the aqueous environment, five temperatures, 5 °C, 15 °C, 25 °C, 40 °C and 50 °C were employed (Fig. 11). Adsorption enthalpy, 5.89 $kJmol^{-1}$, resided within the endothermic range. Adsorption entropy, 64.7 $Jmol^{-1}$ K^{-1}, implied an increase in the random encounter at the adsorbent/solution interface. The Gibbs free energy change were − 12.1 kJ mol^{-1}, −12.7 kJ mol^{-1}, −13.4 kJ mol^{-1}, −14.4 kJ mol^{-1} and -15.0 kJ mol^{-1} at 5 °C, 15 °C, 25 °C, 40 °C and 50 °C respectively. The negative ΔG^0 value showed that the adsorption was spontaneous.

3.8. Recovery

Recovery of a composite adsorbent is for sure one of the economic aspects to be considered. In this study, 0.1 M HCl, NaOH and ethanol solutions were used for the recovery of AO dye from the Ch-K surface. After each experiment, the supernatant was filtered. Then, the remaining AO dye concentration was determined by UV–Vis spectrophotometric method. Five sequential adsorption/desorption experiments were carried out to clarify this feature of Ch-K (Fig. 12). Desorption was studied using HCl or ethanol. The latter chemical yielded much better recovery in activity (88%). Those overall results might shed light on the environmentally-friendly and cost-effective characteristics of the synthesized Ch-K adsorbent.

4. Conclusion

Ch-K, a polymer-mineral composite, was synthesized using two crosslinkers, epichlorohydrin and tripolyphosphate. Both FT-IR- and EDX spectra and also SEM images of the Ch-K proved that the Ch-K synthesis was successful. Adsorption performance of Ch-K for AO dye molecules was optimized: for a dye concentration of 500 mg L^{-1}, the AO quantity was 50 mg, at pH 7.5 at 25 °C. The maximum adsorption capacity of Ch-K, suggested by Langmuir, was 0.118 mol kg^{-1}. D-R isotherms showed that the nature of the adsorption process was physical type and both PSO and IPD models were used to interpret the adsorption

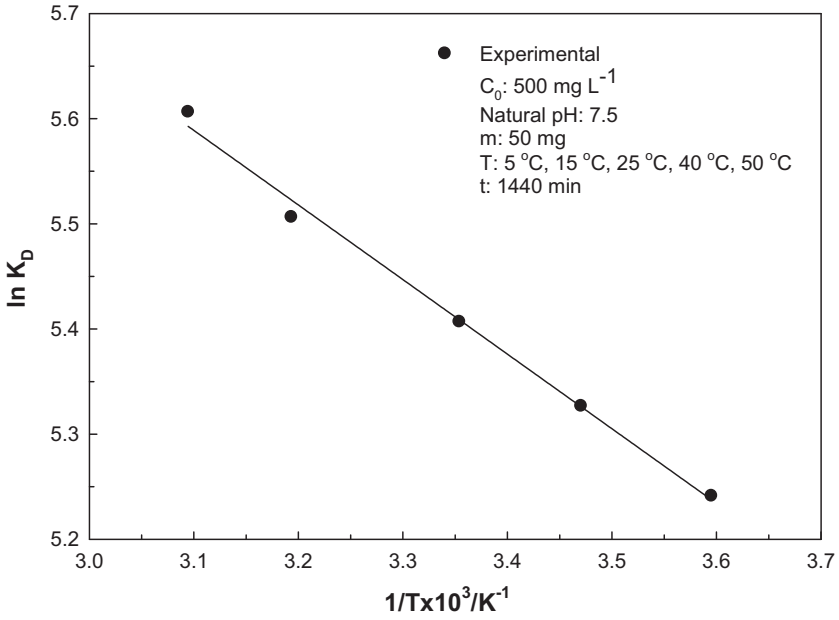

Fig. 11. The effect of temperature on the adsorption.

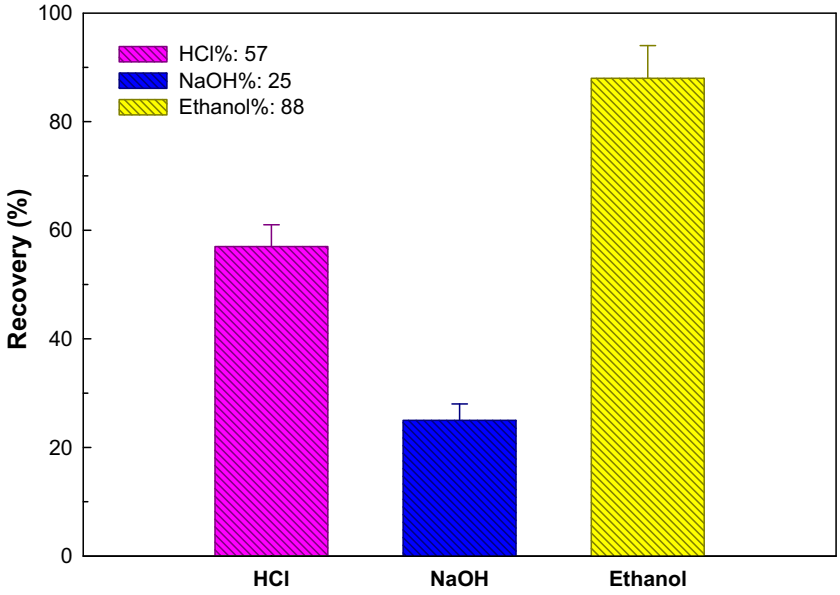

Fig. 12. Recovery of Ch-K.

kinetics. Thermodynamic parameters demonstrated that the adsorption of AO dye on the Ch-K was endothermic and spontaneous. Recovery experiments showed that after five sequential adsorption/desorption cycles, the Ch-K retained its 88% adsorbent activity. Furthermore, the quantum mechanical calculations employed enabled us to propose a first detailed mechanism for the formation of Ch-K. The overall results suggested that Ch-K composite had a remarkable adsorption affinity towards AO dye in aqueous media.

CRediT authorship contribution statement

Zeynep Mine Şenol: Supervision, Investigation, Methodology, Formal analysis, Data curation, Validation, Writing–review & editing, Project administration, **Serap Çetinkaya:** Investigation, Formal analysis. **Ali Fazıl Yenidünya:** Investigation, Formal analysis. **Faika Başoğlu-Ünal:** Investigation, Formal analysis. **Abdulilah Ece:** Supervision, Investigation, Methodology, Formal analysis, Data curation, Validation, Computations, Writing–review & editing.

Acknowledgments

The study was partly supported by Cumhuriyet University Scientific Research Projects Commission. The authors have declared no conflict of interest.

References

[1] V.V. Priyan, T. Shahnaz, A.B. Kunnumakkara, V. Rana, M. Saravanan, S. Narayanasamy, Antioxidant, anti-inflammatory and biosorption properties of starch nanocrystals in vitro study: cytotoxic and phytotoxic, evaluation, J. Clust. Sci. 32 (5) (2021) 1419–1430.
[2] R.A. Rashid, M.A.M. Ishak, K.M. Hello, Adsorptive removal of methylene blue by commercial coconut shell activated carbon, Sci. Lett. 12 (2018) 27–97.
[3] R.A. Rafaie, N.F.M. Yusop, N.F. Azmi, N.I.R. Ramli, Photocatalytic degradation of methylene blue dye solution using different amount of ZnO as a photocatalyst, Sci. Lett. 15 (1) (2021) 1–12.
[4] A.H. Jawaad, A.S. Abdulhameed, E. Kashi, Z.M. Yaseen, Z.A. Alothman, M.R. Khan, Cross-linked chitosan-glyoxal/kaolin clay composite: parametric optimization for color removal and COD reduction of remazol brilliant blue R dye, J. Polym. Environ. (2021) 1–15, https://doi.org/10.1007/s10924-021-02188-1.
[5] S. Tasrin, S.M.M. Fazil, S. Senthilmurugan, N. Selvaraju, Facile preparation of nanocellulose embedded polypyrrole for dye removal: unary and binary process optimization and seed toxicity, Int. J. Environ. Sci. Technol. 18 (2) (2021) 365–378.
[6] V.V. Priyan, T. Shahnaz, E. Suganya, S. Sivaprakasam, S. Narayanasamy, Ecotoxicological assessment of micropollutant diclofenac biosorption on magnetic sawdust: phyto, microbial and fish toxicity studies, J. Hazard. Mater. 403 (2021), 123532.
[7] T. Shahnaz, V.V. Priyan, S. Pandian, S. Narayanasamy, Use of nanocellulose extracted from grass for adsorption abatement of ciprofloxacin and diclofenac removal with phyto, and fish toxicity studies, Environ. Pollut. 268 (2021), 115494.
[8] M. Monier, A.A.H. Bukhari, N.H. Elsayed, Designing and characterization of copper (II) ion-imprinted adsorbent based on isatin functionalized chitosan, Int. J. Biol. Macromol. 155 (2020) 795–804.
[9] M. Monier, D.A. Abdel-Latif, H.A. Mohammed, Synthesis and characterization of uranyl ion-imprinted microspheres based on amidoximated modified alginate, Int. J. Biol. Macromol. 75 (2015) 354–363.
[10] J. Ru, H. Zhu, Y. Fu, Equilibrium and kinetic studies on adsorption of methyl orange from aqueous solution on chitosan/kaolin/Fe2O3 nanocomposite, in: International Conference on Remote Sensing, Environment and Transportation Engineering (RSETE) 24, IEEE, 2011, pp. 7565–7568.
[11] T. Shahnaz, V.V. Priyan, A. Jayakumar, S. Narayanasamy, Magnetic nanocellulose from Cyperus rotundas grass in the absorptive removal of rare earth element cerium (III): toxicity studies and interpretation, Chemosphere 287 (2022), 131912.
[12] H.M.C. Azeredo, D. de Britto, O.B.G. Assis, in: S.P. Davis (Ed.), Chitosan Edible Films and Coatings – A Review, Nova Sci. Publish. Inc, 2011, pp. 179–194.
[13] G. Crini, P.M. Badot, Application of chitosan, a natural aminopolysaccharide, for dye removal from aqueous solutions by adsorption processes using batch studies: a review of recent literature, Prog. Polym. Sci. 33 (2008) 399–447.
[14] H. Zhao, T. Jiao, L. Zhang, J. Zhou, Q. Zhang, Q. Peng, X. Yan, Preparation and adsorption capacity evaluation of graphene oxide chitosan composite hydrogels, Sci. China Mater. 58 (2015) 811–818.
[15] L. Fan, C. Luo, X. Li, F. Lu, H. Qiu, M. Sun, Fabrication of novel magnetic chitosan grafted with graphene oxide to enhance adsorption properties for methyl blue, J. Hazard. Mater. 215–216 (2012) 272–279.
[16] Y. Zhang, S. Chen, X. Feng, J. Yu, X. Jiang, Self-assembly of sponge-like kaolin/chitosan/reduced graphene oxide composite hydrogels for adsorption of Cr(VI) and AYR, Environ. Sci. Pollut. Res. Int. 26 (28) (2019) 28898–28908.
[17] A.H. Jawad, N.N.A. Malek, A.S. Abdulhameed, R. Razuan, Synthesis of magnetic chitosan-fly ash/Fe3O4 composite for adsorption of reactive orange 16 dye; optimization by Box- Behnken design, J. Polym. Environ. 28 (3) (2020) 1068–1082.
[18] N.H. Elsayed, A. Alatawi, M. Monier, Diacetylmonoxine modified chitosan derived ion-imprinted polymer for selective solid-phase extraction of nickel (II) ions, React. Funct. Polym. 151 (2020), 104570.
[19] V. Sharma, T. Shahnaz, S. Subbiah, S., Narayanasamy new insights into the remediation of water pollutants using nanobentonite incorporated nanocellulose chitosan based aerogel, J. Polym. Environ. 28 (7) (2020) 2008–2019.
[20] M. Monier, D.A. Abdel-Latif, Y.G. Abou El-Reash, Ion-imprinted modified chitosan resin for selective removal of pd (II) ions, J. Colloid Interface Sci. 469 (2016) 344–354.
[21] M. Monier, D.A. Abdel-Latif, Fabrication of au (III) ion-imprinted polymer based on thiol-modified chitosan, Int. J. Biol. Macromol. 105 (2017) 777–787.
[22] N.H. Elsayed, R.A. Alatawi, M. Monier, Amidoxime modified chitosan based ion-imprinted polymer for selective removal of uranyl ions, Carbohydr. Polym. 117509 (2021).
[23] W. Bo, E.A. Jackson, J.W. Hoff, P.K. Dutta, Fabrication of zeolite/polymer composite membranes in a roller assembly, Microporous Mesoporous Mater. 223 (2016) 247–253.
[24] K. Lewandowska, A. Sionkowska, B. Kaczmarek, G. Furtos, Characterization of chitosan composites with various clays, Int. J. Biol. Macromol. 65 (2014) 534–541.
[25] Ö. Yavuz, C. Saka, Surface modification with cold plasma application on kaolin and its effects on the adsorption of methylene blue, Appl. Clay Sci. 85 (2013) 96–102.
[26] S.B. Rekik, S. Gassara, J. Bouaziz, A. Deratani, S. Baklouti, Development and characterization of porous membranes based on kaolin/chitosan composite, Appl. Clay Sci. 143 (2017) 1–9.
[27] H.Y. Zhu, R. Jiang, L. Xiao, Adsorption of an anionic azo dye by chitosan/kaolin/γ-Fe2O3 composites, Appl. Clay Sci. 48 (3) (2010) 522–526.
[28] T. Leiviskä, A. Sarpola, J. Tanskanen, Removal of lipophilic extractives from debarking wastewater by adsorption on kaolin or enhanced coagulation with chitosan and kaolin, Appl. Clay Sci. 61 (2018) 22–28.
[29] B. Liu, H. Zheng, Y. Wang, X. Chen, C. Zhao, Y. An, X. Tang, A novel carboxyl-rich chitosan-based polymer and its application for clay flocculation and cationic dye removal, Sci. Total Environ. 640–641 (2018) 107–115.
[30] A. Ece, B. Pejin, A computational insight into acetylcholinesterase inhibitory activity of a new lichen depsidone, J. Enzyme Inhib Med. Chem. 30 (4) (2015) 528–532.
[31] G. Karakuş, A. Ece, A.S. Yaglioglı, H.B. Zengin, M. Karahan, Synthesis, structural characterization, and antiproliferative/cytotoxic effects of a novel modified poly (maleic anhydride-co-vinyl acetate)/doxorubicin conjugate, Polym. Bull. 74 (6) (2017) 2159–2184.
[32] I.H. Tasdemir, A. Ece, E. Kilic, Experimental and theoretical study on the electrochemical behavior of zofenopril and its voltammetric determination, Curr. Pharm. Anal. 8 (4) (2012) 339–348, 8.
[33] Y. Zhao, D.G. Truhlar, The M06 suite of density functionals for main group thermochemistry, thermochemical kinetics, noncovalent interactions, excited states, and transition elements: two new functionals and systematic testing of four M06-class functionals and 12 other functionals, Theor. Chem. Accounts 120 (2008) 2015–2241.
[34] M. Jafari, M.R. Rahimi, M. Ghaedi, H. Javadian, A. Asfaram, Fixed-bed column performances of azure-II and auramine-O adsorption by Pinus eldarica stalks activated carbon and its composite with zno nanoparticles: optimization by response surface methodology based on central composite design, J. Colloid Interface Sci. 507 (2017) 172–189.
[35] M. Monier, N.H. Elsayed, Selective extraction of uranyl ions using ion-imprinted chelating microspheres, J. Colloid Interface Sci. 423 (2014) 113–122.
[36] J. Langmuir, The adsorption of gases on plane surfaces of glass mica and platinum I, J. Am. Chem. Soc. 40 (1918) 1361–1403.
[37] H. Freundlich, Über die adsorption in lösungen, Z. Phys. Chem. 57 (1) (1907) 385–470.
[38] K.Y. Foo, B.H. Hameed, Insights into the modeling of adsorption isotherm systems, Chem. Eng. Sci. 156 (1) (2010) 2–10.
[39] M. Ghasemi, S. Mashhadi, M. Asif, I. Tyagi, S. Agarwal, V.K. Gupta, Microwaveassisted synthesis of tetraethylenepentamine functionalized activated carbon with high adsorption capacity for malachite green dye, J. Mol. Liq. 213 (2016) 317–325.
[40] Y.S. Ho, G. McKay, Pseudo-second order model for sorption processes, Process Biochem. 34 (5) (1999) 451–465.
[41] W.J. Weber Jr., J.C. Morris, Kinetics of adsorption on carbon from solution, J. Sanit. Eng. Div. 89 (2) (1963) 31–59.
[42] M. Monier, D.A. Abdel-Latif, Synthesis and characterization of ion-imprinted resin based on carboxymethyl cellulose for selective removal of UO22+, Carbohydr. Polym. 97 (2) (2013) 743–752.
[43] Y.S. Ho, A.E. Ofomaja, Pseudo-second-order model for lead ion sorption from aqueous solutions onto palm kernel fiber, J. Hazard. Mater. 129 (2006) 137–142.
[44] E.C. Lima, A. Hosseini-Bandegharaei, J.C. Moreno-Piraján, I. Anastopoulos, A critical review of the estimation of the thermodynamic parameters on adsorption equilibria. Wrong use of equilibrium constant in the Van't hoof equation for calculation of thermodynamic parameters of adsorption, J. Mol. Liq. 273 (2019) 425–434.
[45] A. Pawlak, M. Mucha, Thermogravimetric and FTIR studies of chitosan blends, Thermochim. Acta 396 (2003) 153–166.
[46] A.T. Paulino, J.I. Simionato, J.C. Garcia, J. Nozaki, Characterization of chitosan and chitin produced from silkworm crysalides, Carbohydr. Polym. 64 (1) (2006) 98–103.
[47] A. Kumar, P. Lingfa, Sodium bentonite and kaolin clays: comparative study on their FT-IR, XRF, and XRD, Mater. Today: Proc. 22 (2020) 737–742.
[48] Y. Kara, S. Sagdinc, A. Esme, Theoretical study on the relationship between the molecular structure and corrosion inhibition efficiency of long alkyl side chain acetamide and isoxazolidine derivatives, Protect. Metals Phys. Chem. Surf. 48 (2012) 710–721.
[49] Y. Cao, R.E. Malekshah, Z. Heidari, R. Pelalak, A. MArjani, S. Shirazian, Molecular dynamic simulations and quantum chemical calculations of adsorption process using amino-functionalized silica, J. Mol. Liq. 330 (2021) 115544.
[50] Z. Heidari, R. Pelalak, R.E. Malekshah, M. Pishnamazi, A. Marjani, S.M. Sarkar, S. Shirazian, Molecular modeling investigation on mechanism of cationic dyes removal from aqueous solutions by mesoporous materials, J. Mol. Liq. 329 (2021) 115485.
[51] A. Ece, B. Pejin, A computational insight into acetylcholinesterase inhibitory activity of a new lichen depsidone, J. Enzyme Inhib. Med. Chem. 30 (4) (2015) 528–532.
[52] M. Monier, D.A. Abdel-Latif, I. Youssef, Preparation of ruthenium (III) ion-imprinted beads based on 2-pyridylthiourea modified chitosan, J. Colloid Interface Sci. 513 (2018) 266–278.
[53] M. Firoozi, Z. Rafiee, K. Dashtian, New MOF/COF hybrid as a robust adsorbent for simultaneous removal of auramine O and rhodamine B dyes, ACS Omega 5 (16) (2020) 9420–9428.
[54] S. Chaudhary, J. Sharma, B.S. Kaith, S. Yadav, A.K. Sharma, A. Goel, Gum xanthan-psyllium-cl-poly(acrylic acid-co-itaconic acid) based adsorbent for effective

removal of cationic and anionic dyes: adsorption isotherms, kinetics and thermodynamic studies, Ecotoxicol. Environ. Saf. 149 (2018) 150–158.
[55] M. Mangla, G. Meenakshi, G.R. Chaudhary, M.L. Sharma, Equilibrium and thermodynamics of auramine-O adsorption from aqueous solution by activated carbons, J. Appl. Chem. 3 (4) (2014) 1719–1726.
[56] M. Abdolhosseinzadeh, S.J. Peighambardoust, H. Erfan-Niya, P.M. Pakdel, Swelling and auramine-O adsorption of carboxymethyl cellulose grafted poly (methyl methacrylate)/Cloisite 30B nanocomposite hydrogels, Iran. Polym. J. 27 (10) (2018) 807–818.
[57] S.E. Karekar, K.A. Gondhalekar, D.K. Sonawane, D.V. Pinjari, Acoustic cavitation assisted preparation of poly (acrylic acid)-halloysite nanoclay hydrogel for removal of auramine o dye from effluent, Curr. Environ. Eng. 5 (1) (2018) 47–57.
[58] R.W. Gaikwad, S.A.M. Kinldy, Studies on auramine dye adsorption on psidium guava leaves, Korean J. Chem. Eng. 26 (1) (2009) 102–107.
[59] V.K. Singh, A.B. Soni, R.K. Singh, Auramine „O" dye adsorption onto de-oiled cotton seed cake biochar: process optimization using response surface methodology for maximizing adsorbate removal, Int. J. ChemTech Res. 9 (7) (2016) 340–353.
[60] T. Mahmud, Biosorption of auramine O and drimarene dyes from aqueous solutions using seed powder of Diospyros lotus, Int. J. Environ. Sustain. 6 (3) (2018).
[61] I.D. Mall, V.C. Srivastava, N.K. Agarwal, Adsorptive removal of auramine-O: kinetic and equilibrium study, J. Hazard. Mater. 143 (1–2) (2007) 386–395.